J Neuropathol Exp Neurol
Vol. 77, No. 7, July 2018, pp. 555–566
doi: 10.1093/jnen/nly031

OXFORD

ORIGINAL ARTICLE

Correlating Clinical Risk Factors and Histological Features in Ruptured and Unruptured Human Intracranial Aneurysms: The Swiss AneuX Study

Sandrine Morel, PhD, Mannekomba R. Diagbouga, MSc, Nicolas Dupuy, Esther Sutter, Vincent Braunersreuther, PhD, Graziano Pelli, Marco Corniola, MD, Renato Gondar, MD, Max Jägersberg, MD, Nathalie Isidor, Karl Schaller, MD, Marie-Luce Bochaton-Piallat, PhD, Philippe Bijlenga, MD-PhD, and Brenda R. Kwak, PhD

Abstract

Pathogenesis of intracranial aneurysm is complex and the precise biomechanical processes leading to their rupture are uncertain. The goal of our study was to characterize the aneurysmal wall histologically and to correlate histological characteristics with clinical and radiological factors used to estimate the risk of rupture. A new biobank of aneurysm domes resected at the Geneva University Hospitals (Switzerland) was used. Histological analysis revealed that unruptured aneurysms have a higher smooth muscle cell (SMC) content and a lower macrophage content than ruptured domes. These differences were associated with more collagen in unruptured samples, whereas the elastin content was not affected. Collagen content and type distribution were different between thick and thin walls of unruptured aneurysms. Classification of aneurysm domes based on histological characteristics showed that unruptured samples present organized wall rich in endothelial and SMCs compared with ruptured samples. Finally, aneurysm wall composition was altered in unruptured domes of patients presenting specific clinical factors used to predict rupture such as large dome diameter, dome irregularities, and smoking. Our study shows that the wall of aneurysm suspected to be at risk for rupture undergoes structural alterations relatively well associated with clinical and radiological factors currently used to predict this risk.

From the Department of Pathology and Immunology, Faculty of Medicine, University of Geneva, Geneva, Switzerland (SM, MRD, ND, ES, GP, MLBP, BRK); Neurosurgery Division, Department of Clinical Neurosciences, Faculty of Medicine, Geneva University Hospitals, Geneva, Switzerland (SM, ND, MC, RG, MJ, NI, KS, PB); Department of Clinical Pathology, Faculty of Medicine, University of Geneva and Geneva University Hospitals, Geneva, Switzerland (VB); Clinical Trial Unit, Faculty of Medicine, Geneva University Hospitals, Geneva, Switzerland (NI); and Department of Medical Specializations – Cardiology, Faculty of Medicine, University of Geneva, Geneva, Switzerland (BRK).

Send correspondence to: Sandrine Morel, PhD, Department of Pathology and Immunology, Centre Médical Universitaire, Rue Michel-Servet, 1 F06.2767.a, 1211 Geneva, Switzerland; E-mail: sandrine.morel@unige.ch

This study was supported by grants from the Swiss SystemsX.ch initiative, evaluated by the Swiss National Science Foundation (to PB and BRK) and the Foundation Carlos et Elsie De Reuter (to BRK and PB).

The authors have no duality or conflicts of interest to declare.

Key Words: Collagen, Endothelial cells, Intracranial aneurysm, Risk factors, Smooth muscle cells, Wall thickness.

INTRODUCTION

Intracranial aneurysm (IA) formation results from the deformation and the enlargement of the arterial lumen. IAs are mostly quiescent and asymptomatic but their rupture induces severe brain damage and death. The prevalence of IAs is high (2%–5%) and they most frequently affect middle-aged females (median at 50 years). The incidence of IA rupture is estimated at 9/100 000 inhabitants per year in western populations (1). In Switzerland, IA rupture results in 13.3% patients recovering with no residual symptoms, 54% patients getting back to an independent life, 31% severely disabled patients, and 15% death (2). One third of the patients suffer from multiple IAs. The risk of rupture is associated with factors of the IA itself such as location, size or presence of dome irregularities, and patient-related factors including ethnicity, age, hypertension, or smoking (3–7).

As may be predicted from the discrepancy between the high prevalence of IAs and the low incidence of IA rupture, subarachnoid hemorrhage (SAH) will not occur during the lifetime of 50% of the patients diagnosed with an IA (1). Treatment of unruptured IAs requires a perilous intervention that induces patient's disability for several months (5%–7% morbidity) and also death in the worst case (1%–4% mortality) (8–10). As an increasing number of patients face the need to decide whether or not to risk an intervention, it is extremely important to better define the characteristics of rupture-prone IAs, and to find appropriate clinical and radiological markers to determine IA rupture risk.

The pathogenesis of IA formation and growth is complex and the precise biomechanical processes leading to IA wall rupture are not yet known. Several studies have shown that lack of internal elastic lamina, erosion of luminal endothelium, infiltration of inflammatory cells, loss of smooth muscle cells (SMCs), destruction of the extracellular matrix (ECM),

activation of the innate immunity, calcification, or lipid accumulation are associated with IA wall degeneration and rupture (11–16). Although these studies have increased our knowledge on aneurysm wall characteristics, these isolated postsurgical observations have been of limited help for the clinician to predict whether an IA should be treated or not. There remains an urgent need for diagnostic markers to estimate the risk of IA rupture. The goal of our study was to characterize the aneurysmal wall histologically and to directly correlate histological features with clinical and radiological factors classically used to estimate the risk of IA rupture. In the context of the AneuX project (17), a new biobank of ruptured IA (R-IA) and unruptured IA (UR-IA) domes resected during neurosurgical clipping at the Geneva University Hospitals in Switzerland was used.

MATERIALS AND METHODS

Clinical and Radiological Data

Patients have been recruited at the Geneva University Hospitals. The inclusion criteria were as follows: 1) IA identified on the basis of angiographic appearance (3D-Digital Subtraction Angiography [3D-DSA], 3D-Magnetic Resonance Angiogram [3D-MRA], or 3D-Computed Tomography Angiogram [3D-CTA]) as well as availability of surgical documentation; 2) age older than 18 years; and 3) patient to provide informed consent. The exclusion criteria were as follows: 1) lack of angiographically proven IA on 3D-DSA, 3D-MRA, or 3D-CTA; 2) failure to contribute to clinical data; 3) age younger than 18 years; and 4) refusal to provide informed consent. The study was approved by the Ethical Committee of the Geneva University Hospitals, Geneva, Switzerland (Geneva Local Ethical Authorization reference CER 07-056 [NAC 07-020, @neurIST (18)]). All patients consented their data and biological samples to be used for research in the field of cerebrovascular diseases according to the information and consent forms. Procedures were in accordance with the Helsinki Declaration of the World Medical Association.

For all recruited patients, available baseline characteristics were collected including: 1) Age of the patient when IA was discovered or when IA ruptured; 2) Sex of the patient; 3) Clinical history for IA: (i) presence of multiple IAs; (ii) previous aneurysmal SAH from another IA or from the same IA; (iii) positive familial history for IA: one or more 1st degree relative(s) with IA; 4) Risk factors for IA: smoking status defined as (i) never smoked: never smoked >300 cigarettes ever; (ii) current smoker: smoked >300 cigarettes and continues current smoking; (iii) former smoker: smoked >300 cigarettes and stopped at least 6 months ago. Arterial hypertension is defined as blood pressure >140/90 mmHg independently of the existence or not of a treatment against hypertension; 5) For patients with SAH, the time between the first signs of rupture and the resection of the IA has been estimated as precisely as possible, and 2 periods were defined, that is, <2 days and >2 days.

On the basis of images obtained from 3D-MRA, 3D-CTA, and 3D-DSA, IA location was determined, IA morphological information such as presence of submillimetric irregularities (roughness), single or multiple blebs or lobules were obtained, and neck size and maximal dome diameter were measured, as previously described (19, 20).

Human Saccular IA Samples

Human saccular IA samples were obtained during microsurgery by resecting the aneurysmal dome after clipping of the aneurysmal neck (Fig. 1A–C). All samples were collected at the neurosurgery division of the Geneva University Hospitals and were stored following 2 different routines depending on the timing of IA resection. Four R-IAs and 8 UR-IAs stored in RNAlater stabilization solution (Qiagen, Hombrechtikon, Switzerland) at −80°C for several months were gently thawed on ice, fixed for 2 hours in formol and embedded in paraffin. Thirteen R-IAs and 23 UR-IAs were directly fixed in formol and stored at room temperature until embedding in paraffin. The percentage of samples stored in RNAlater stabilization solution was 24% in the ruptured group and 26% in the unruptured group. Detailed histological assessment of the tissue integrity associated with both routines showed that samples from both groups were similar. For example, intact nuclei were readily observed by hematoxylin and eosin staining in samples conserved in RNAlater stabilization solution (Fig. 1D, G) and in samples directly fixed in formol (Fig. 1J, M). Moreover, antibody-based immunohistological staining (see below) resulted in similar positive labeling between the 2 protocols (Fig. 1E, H, K, N as examples for α-smooth muscle actin [α-SMA] staining). Finally, histological staining performed to reveal the ECM showed equivalent patterns between the 2 methods (Fig. 1F, I, L, O as examples for Masson-trichrome staining).

Histology and Immunohistochemistry

IA domes were embedded in paraffin, sectioned at 5 μm and conserved at 4°C. For histology, aneurysmal dome sections were stained routinely with hematoxylin and eosin, Masson-trichrome (total collagen), Victoria blue (elastin) and with Picrosirius Red (type I and III collagen; Sigma–Aldrich, Buchs, Switzerland). For immunohistochemistry, sections were immunolabeled with antibodies recognizing α-SMA (mouse IgG2a antibody, clone 1A4 (21, 22); a general marker of SMCs), smooth muscle myosin heavy chains (SMMHC) types 1 and 2 (rabbit polyclonal antibody, BT-562, Biomedical Technologies, Inc., Stoughton, MA; a marker of well-differentiated SMCs), CD68 (mouse IgG1 antibody, clone KP1, Dako, Glostrup, Denmark; marker of macrophages), or CD31 (rabbit polyclonal antibody, clone pAK, Dianova, Hamburg, Germany; a marker of endothelial cells). Before using the first antibody, immunoreactivity was retrieved by microwave treatment (600 W, 5 minutes) in citrate buffer (10 mM, pH 6.0) for α-SMA and CD68, and by pressure cooker treatment (3 minutes) in citrate buffer for SMMHCs and CD31. Goat antimouse- or antirabbit-biotinylated IgGs (Dako) were used as secondary antibodies and the streptavidin-biotin peroxidase complex and 3, 3′-diamino-benzidine chromophore were used for visualization (EnVision system; Dako).

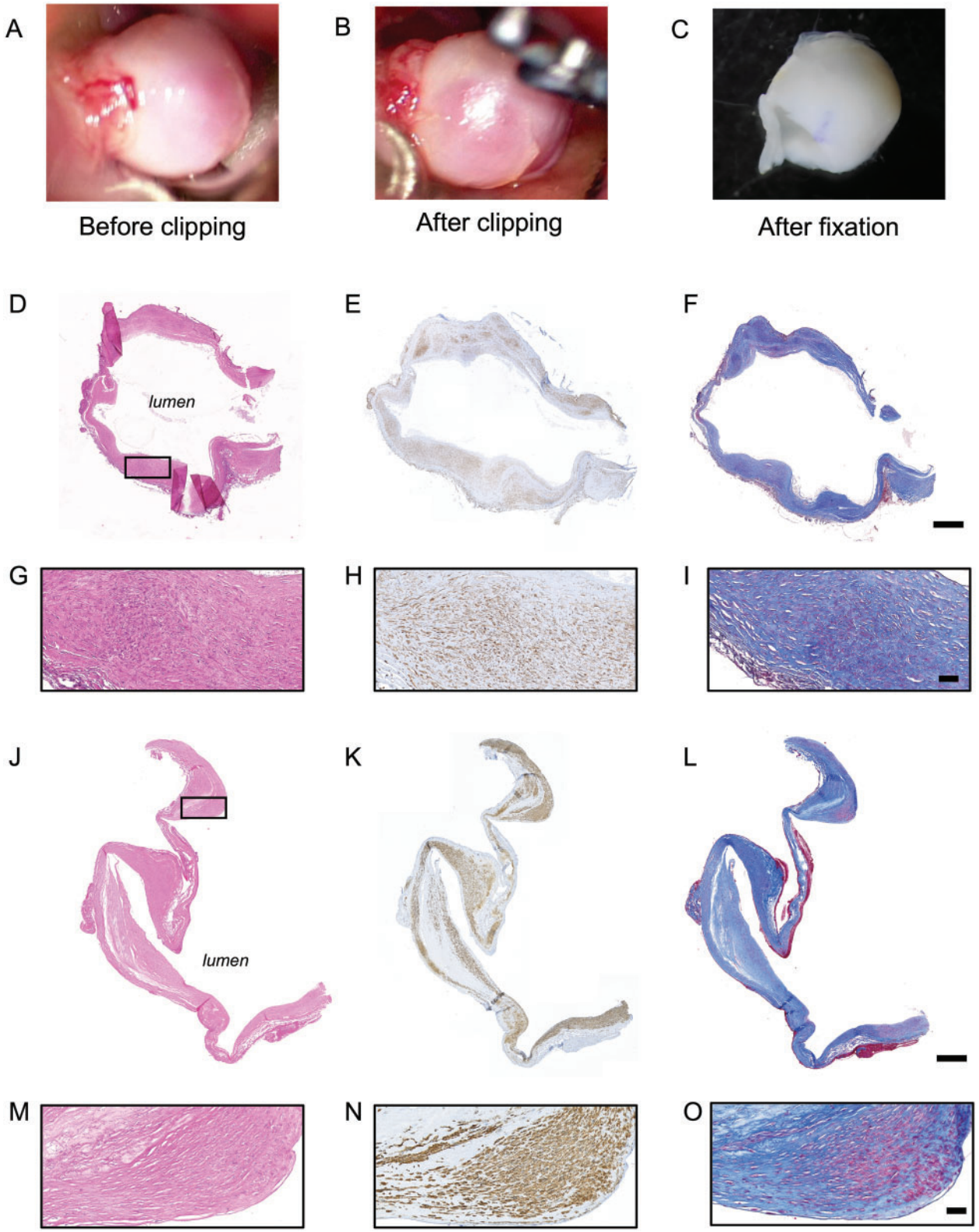

FIGURE 1. Sample preparation. Examples of intracranial aneurysm (IA) dome obtained during the surgery (before **[A]** and after **[B]** the clipping of the IA neck) and just before paraffin embedding **(C)**. Representative examples of H&E **(D, G, J, M)**, α-SMA (SMCs in brown, **E**, **H**, **K**, **N**) and Masson-trichrome (collagen in blue, **F**, **I**, **L**, **O**) stainings performed on IA domes stored in RNA latter solution **(D–I)** or directly fixed in formol **(J–O)**. The black rectangle in panels **D** and **J** represent the region of magnification for panels **G–I** and **M–O**. Scale bars: **D-F**, **J-L** = 500 μm; **G-I**, **M-O** = 50 μm.

Hemalun (Merck, Darmstadt, Germany) was used as counterstaining. All stainings were performed on consecutive sections.

Image Analyses

Sections were scanned at 10× magnification and high resolution using the fully automated slide scanner Axioscan.Z1 (Carl Zeiss Microscopy, Oberkochen, Germany) and images were processed using the software ZEN 2 (Carl Zeiss Microscopy). Depending on the size of the sample, 3–5 regions of interest (ROI) were manually determined for all aneurysms to cover almost the entire surface of the sample. The size of these ROIs was always identical (0.48 μm^2) and the ROI was placed at the same regions inside each aneurysm for the different stainings. Total tissue area and positive area in each ROI were quantified using the NIH Image software (NIH AutoExtractor 1.51; National Institutes of Health, Bethesda, MD) and the positive staining was expressed as a percentage of the total area. Results were calculated as the mean of the 3–5 ROIs for each staining.

To evaluate the relative contribution of type I and type III collagen in the aneurysm wall, sections stained with Picrosirius red were examined using polarized light on a Zeiss Axioskop 2 plus microscope and images were processed using the software AxioVision 4.8.10. Yellow-red birefringence and green birefringence were used to discriminate between type I and type III collagen fibers, respectively. As for all other stainings, total tissue area and positive area were quantified using the NIH Image software and the positive staining was expressed as a percentage of the total area. Results were calculated as the mean of the 3–5 ROIs.

To quantify endothelial cell coverage, using the NIH Image software, we determined the length of the intraluminal part positively stained for CD31 as a percentage of the total length of the intraluminal part of the resected dome.

Statistical Analyses

We calculated that a minimum of 16 IAs/group were needed to see a significant difference of 40% between the 2 groups with a significance level of 5% and a power of 90%. Results are shown in median (interquartile range), in percentage or in correlation. Comparisons of medians have been performed using a nonparametric Mann-Whitney *U* test. Comparisons of distributions have been performed using the Fisher exact test or Chi-square test. Spearman correlations were performed to examine association between variables. Differences were considered statistically significant at values of $p \leq 0.05$.

RESULTS

Patient and IA Characteristics

Patients with ruptured (n = 17) and unruptured (n = 30) IAs did not differ in age, sex, ethnicity, presence of multiple IAs, existence of a previous aneurysmal SAH, positive familial history for IA or SAH, smoking status or hypertension (Table 1). IA characteristics just before the surgery, that is, location, presence of irregularities (roughness, blebs, and lobules), neck size, and maximal dome diameter, were not different between R-IAs and UR-IAs (Table 2).

TABLE 1. Patient Characteristics at the Time of the Inclusion in the Study

	Ruptured IAs	Unruptured IAs	p value
Patients	n = 17	n = 30	
Age, years: median (IQR)	55 (44–64)	53 (44–64)	0.83
Sex, female: n (%)	14 (82)	22 (73)	0.72
Ethnicity: Eurasian: n (%)	15 (88)	30 (100)	0.13
Multiple aneurysms: n (%)	7 (41)	19 (63)	0.35
Previous aSAH: n (%)	1 (6)	4 (26)	0.64
Positive familial history for IA: n (%)	2 (12)	6 (23)	0.69
Smoker (former and current): n (%)	10 (59)	20 (67)	0.31
Hypertension: n (%)	5 (29)	15 (50)	0.35

Comparisons of medians and percentages have been performed using nonparametric Mann-Whitney *U* test or Fisher exact test, respectively.

Positive familial history for IA is defined as one or more 1st degree relative(s) with IA.

A current smoker is a patient currently smoking >300 cigarettes and a former smoker is a patient who smoked >300 cigarettes and who stopped at least 6 months ago.

Arterial hypertension is defined as blood pressure >140/90 mmHg independently of the existence or not of a treatment against hypertension.

ECM Content

Collagen content in IA wall was determined using 2 different staining protocols: Masson-trichrome allowing us to visualize total collagen in blue as well as Picrosirius red followed by polarized light examination to distinguish type I collagen fibers (in yellow-red) and type III collagen fibers (in green). We found that R-IAs contained less collagen (total, type I and type III) than UR-IAs (Fig. 2A–E). The relative contribution of type I and III collagens was similar between the 2 groups (Fig. 2F). In contrast to collagen content, the elastin content was not different between R-IAs and UR-IAs (Fig. 2G–H).

To determine whether the content in ECM was influenced by the thickness of the IA wall, we compared thick (tissue area >0.31 μm^2 in the defined ROI) to thin (tissue area <0.31 μm^2 in the defined ROI) aneurysmal wall regions. The cut-off of 0.31 μm^2 was chosen based on the mean tissue area in the defined ROI of all samples. Thick regions had similar mean area values between R-IAs and UR-IAs ($0.41 \pm 0.03\ \mu m^2$ and $0.39 \pm 0.06\ \mu m^2$, respectively). Similarly, mean areas of thin regions were also not different between R-IAs and UR-IAs ($0.21 \pm 0.08\ \mu m^2$ and $0.18 \pm 0.06\ \mu m^2$, respectively). Thin regions of UR-IAs appeared to contain less total collagen than thicker regions (Fig. 3A), whereas total collagen content was not affected by the thickness of the IA wall in the ruptured group (Fig. 3F). The relative contribution of type I and type III collagens between thin and thick regions in UR-IAs was significantly different (Fig. 3B) due to a higher content of type I collagen (Fig. 3C) and a lower content of type III collagen in the thin IA wall regions (Fig. 3D). In R-IAs, type I and type III collagen contents (Fig. 3H, I) and relative contribution (Fig. 3G) were not

TABLE 2. Intracranial Aneurysm Characteristics Before Surgery

	Ruptured IAs	Unruptured IAs	p value
Intracranial aneurysm	n = 17	n = 31	
Location: n (%)	MCA: 11 (65) ACA: 4 (23) ICA: 1 (6) Unknown: 1 (6)	MCA: 24 (77.5) ACA: 6 (19.5) ICA: 1 (3)	0.75
Rough appearance: n (%)	4 (22)	14 (45)	0.33
Presence of blebs or lobules: n (%)	9 (53)	18 (58)	0.75
Neck size, mm: median (IQR)	3.8 (2.4–4.4)	3.6 (3.0–5.0)	0.54
Maximal diameter, mm: median (IQR)	7.5 (6.2–10.5)	6.2 (4.5–9.3)	0.27
Time from rupture to resection: n	<2 days: 10 >2 days: 6 Unknown: 1	NA	–

Comparisons of medians and percentages have been performed using nonparametric Mann-Whitney *U* test or Fisher exact test, respectively.

Rough appearance is defined as the presence of submillimetric irregularities.

IQR = interquartile range; ICA= internal carotid artery; MCA = middle cerebral artery; ACA = anterior cerebral arteries, including: anterior cerebral artery, anterior communicating artery (Acom) and pericallosal artery (A2); n, number; NA: not applicable.

different between thin and thick regions. Total, type I and type III collagen contents were significantly lower in thick regions of R-IAs in comparison to thick regions of UR-IAs ($p < 0.001$, $p < 0.05$, and $p < 0.01$, respectively). Thin regions of R-IAs had a lower content of type I collagen ($p < 0.01$) whereas the content in type III collagen was not different between the 2 groups. Finally, elastin content was similar between thick and thin regions of UR-IAs (Fig. 3E) or R-IAs (Fig. 3J).

Cellular Content

Presence of endothelial cells (CD31-positive cells) was found in 9 R-IAs out of the 17 samples harvested for this group, and in 26 UR-IAs over the 31 harvested for this group ($p < 0.05$). The percentage of endothelial coverage of the IA wall varied from 7.1% to 52.8% in the ruptured group and from 2.2% to 91.1% in the unruptured group. The wall of UR-IAs contained more total and differentiated SMCs (α-SMA and SMMHCs staining, respectively) than the wall of R-IAs (Fig. 4A–D) but the proportion of differentiated SMCs was not different between the 2 groups (32% and 35% in R-IAs and UR-IAs, respectively, ns). Moreover, the UR-IA walls presented a significantly lower content of inflammatory CD68-positive cells in comparison to R-IAs (Fig. 4E, F). Subsequently, 2 subgroups have been compared in the ruptured group; a first subgroup in which the time between the first signs of rupture and the resection of the aneurysm has been estimated lower than 2 days (n = 10) and a second group in which this time has been estimated longer than 2 days (n = 6) (Table 2). The time between the first signs of rupture and the resection was unknown for 1 patient. The percentage of CD68-positive cells was not different between the 2 subgroups (median [interquartile range]: <2 days = 2.2 (0.3–3.6); >2 days = 5.2 (1.1–7.2), ns). However, the percentage of CD68-positive cells present in recently ruptured domes (<2 days) was significantly higher in comparison to UR-IA domes (0.4 [0–1.1], $p < 0.01$, nonparametric Mann-Whitney *U* test). Finally, we found no correlations between cellular content (CD68-positive cells or α-SMA-positive cells) and collagen content within the walls of ruptured (Fig. 4G, H) or unruptured (Fig. 4I, J) IAs. In contrast to collagen content, α-SMA, SMMHCs, and CD68 contents were not different between thick and thin regions in the UR-IAs (Fig. 4K–M). Moreover, we observed no difference with respect to these 3 markers between thick and thin regions in R-IAs (data not shown).

IA Wall Classification

IA domes obtained after surgical clipping in Finland have been elegantly classified according to histological severity grades based on the following definitions (12): (a) Endothelialized wall with linearly organized SMCs; (b) Thickened wall with disorganized SMCs; (c) Hypocellular wall with either intimal hyperplasia or organizing luminal thrombosis; and (d) An extremely thin thrombosis-lined hypocellular wall.

We classified the 48 Swiss IA domes according the above criteria (see Fig. 5A for examples). Using the dominant wall type observed in the resected sample (i.e. the wall type covering the vast majority of the dome surface), 16%, 55%, 26%, and 3% of UR-IA domes were classified as a, b, c, and d, respectively (Fig. 5B). Interestingly, the percentage of R-IA domes for each histological severity grade was 0%, 18%, 70%, and 12%, respectively, demonstrating a significant difference in the distribution of histological severity grades between both groups (Fig. 5B). Thus, the group of UR-IAs was populated with a majority of a and b grades representing the relatively organized IA wall types, whereas the ruptured group contained mainly c and d wall severity grades. When we based our classification of the IA domes on the most severe focal histological grade observed within the IA dome sample, 26%, 42%, and 32% of UR-IA domes were graded b, c, and d, respectively, which is significantly different from the distribution obtained in R-IAs (b: 12%, c: 76%, d: 12%) (Fig. 5C). Finally, a direct comparison of the 2 grading methods showed that in the ruptured group, the classification of IA wall based on the dominant wall type or in the most pathological score was not different, whereas the distribution was significantly different in the unruptured group (Fisher exact test, $p < 0.001$).

Aneurysmal Wall Composition and Clinical Risk Factors for Rupture

IA Size

Increased size of UR-IAs correlated with a higher content of CD68-positive cells (Fig. 6A) and total collagen (Fig. 6B), more particularly with type III collagen (Fig. 6C).

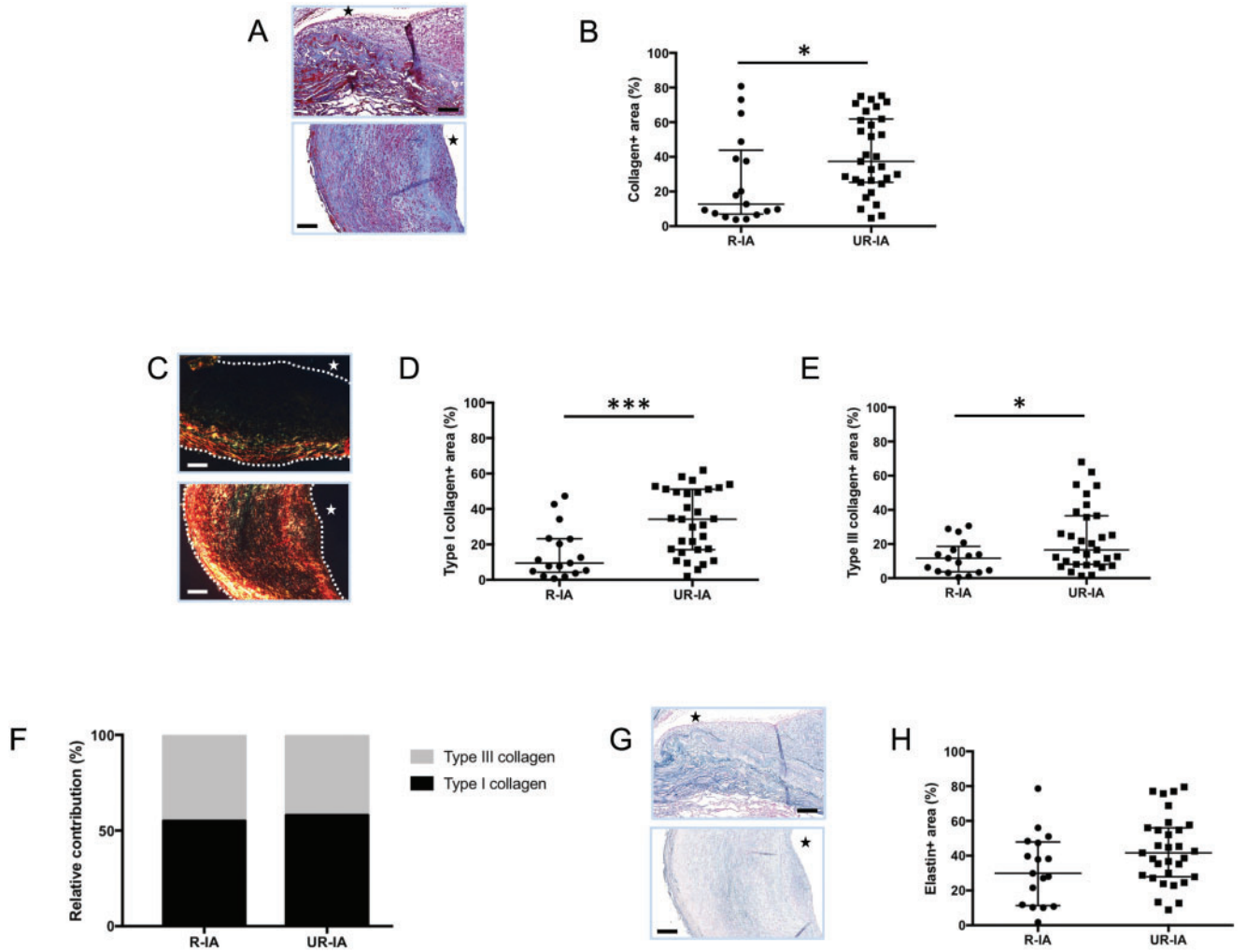

FIGURE 2. Extracellular matrix composition in ruptured and unruptured intracranial aneurysms (IAs). Representative examples and quantification of total collagen (Masson-trichrome staining: collagen in blue, **A, B**), type I collagen (Picrosirius red staining: type I collagen in yellow-red, **C, D**) and type III collagen (Picrosirius red staining: type III collagen in green, **C, E**) in ruptured (R-IA) and unruptured (UR-IA) IA domes. The relative contribution of type I (black) and type III (grey) collagen is not different between the 2 groups **(F)**. Representative examples and quantification of elastin (Victoria blue staining: elastin in blue, **G, H**) in ruptured and unruptured IA domes. The lumen of the vessel is indicated by a star. Scale bars in panels **A**, **C**, and **G** represent 100 μm. Dotted lines on the images of panel C represent the borders of the samples. Results are shown as individual values and as median ± interquartile range **(B, D, E,** and **H)** or in percentage **(F)**. *$p < 0.05$, ***$p < 0.001$, nonparametric Mann-Whitney *U* test.

However, we found no correlation between the size of UR-IAs and SMC or elastin content (data not shown).

Dome Irregularity

UR-IA domes with submillimetric irregularities (rough) contained more type III collagen in comparison to IAs with a smooth appearance (Fig. 6D). The amount of type I collagen was not different between rough and smooth domes, which led to a significantly lower ratio type I collagen/type III collagen for rough domes (Fig. 6E). Presence or absence of irregularities (roughness, blebs or lobules) was not significantly associated with any other aneurysmal wall characteristic (data not shown).

Smoking Status

Analysis of the association of clinical risk factors for IA rupture and histological characteristics of UR-IAs wall revealed that the aneurysmal wall of smokers contains less SMCs in comparison to the wall of nonsmokers (Fig. 6F). Intriguingly, the reduced SMC content in the IA wall of smokers was similar to that measured in R-IAs (Fig. 6F). Finally, classification of UR-IA domes per most severe focal histological grades for smokers and nonsmokers resulted in 19% (b), 48% (c), and 33% (d) versus 40%, 30%, and 30%, respectively (Chi-square test, $p < 0.01$). Smoking status was not correlated with others histological characteristics of the IA wall (data not shown). Finally, we found no association

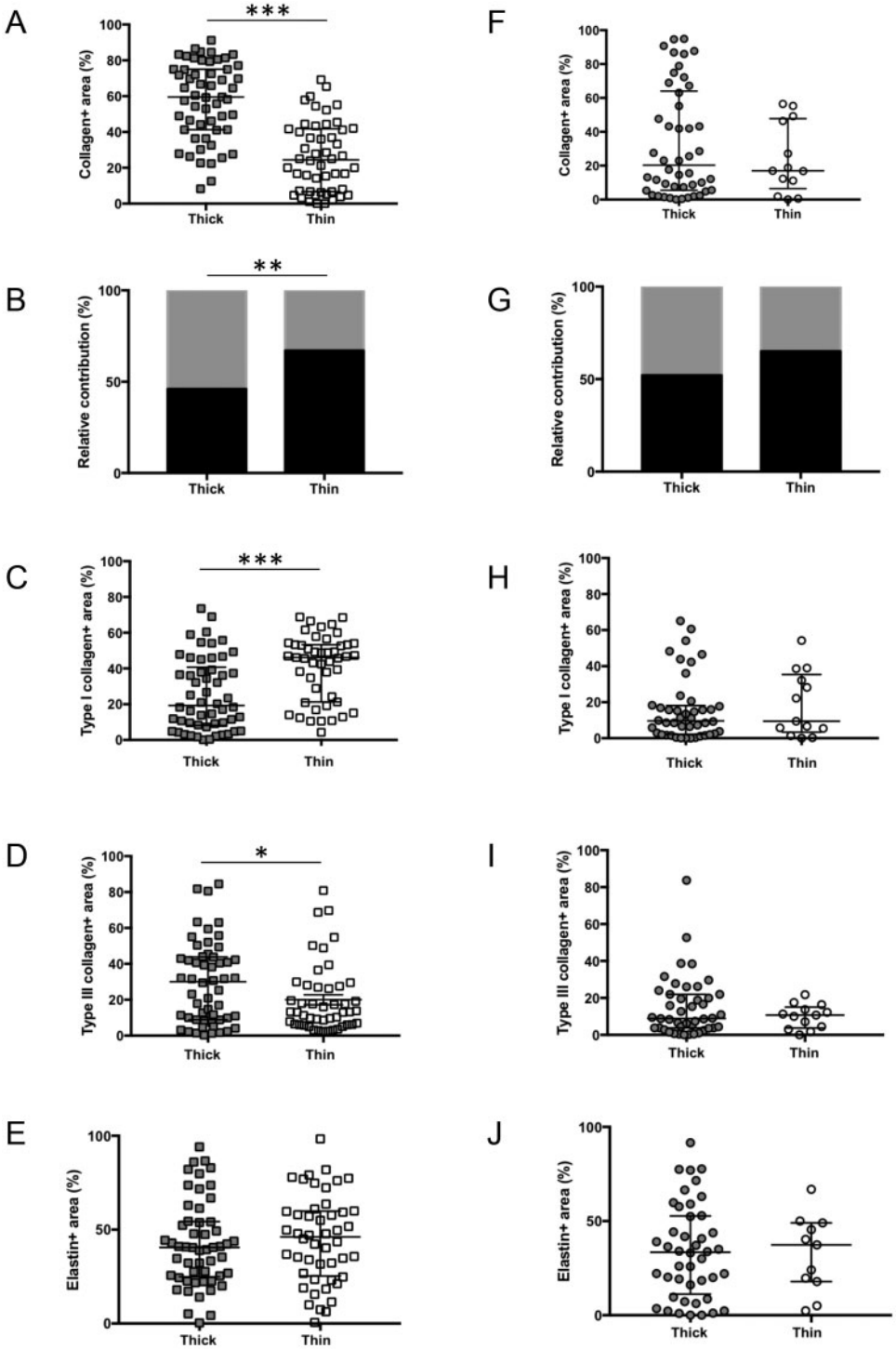

FIGURE 3. Extracellular matrix composition and thickness of intracranial aneurysm (IA) wall. Thin regions of UR-IAs contain less total collagen than thicker regions **(A)**, whereas total collagen content is not affected by the thickness of the IA wall in the ruptured group **(F)**. Type I (black) and III (grey) collagen relative contributions are significantly different between thick and thin regions of UR-IA domes **(B)** due to a higher content of type I collagen **(C)** and a lower content in type III collagen **(D)** in thin regions. No significant differences have been found for these parameters in R-IAs **(G–I)**. Elastin content is not influenced by the thickness of aneurysmal wall in UR-IA **(E)** and R-IA **(J)** domes. Results are shown as individual values and as median ± interquartile range **(A, C–F, H–J)** or in percentage **(B, G)**. *$p < 0.05$, **$p < 0.01$, ***$p < 0.001$, nonparametric Mann-Whitney *U* test for comparison of median and Fisher exact test for comparison of distributions.

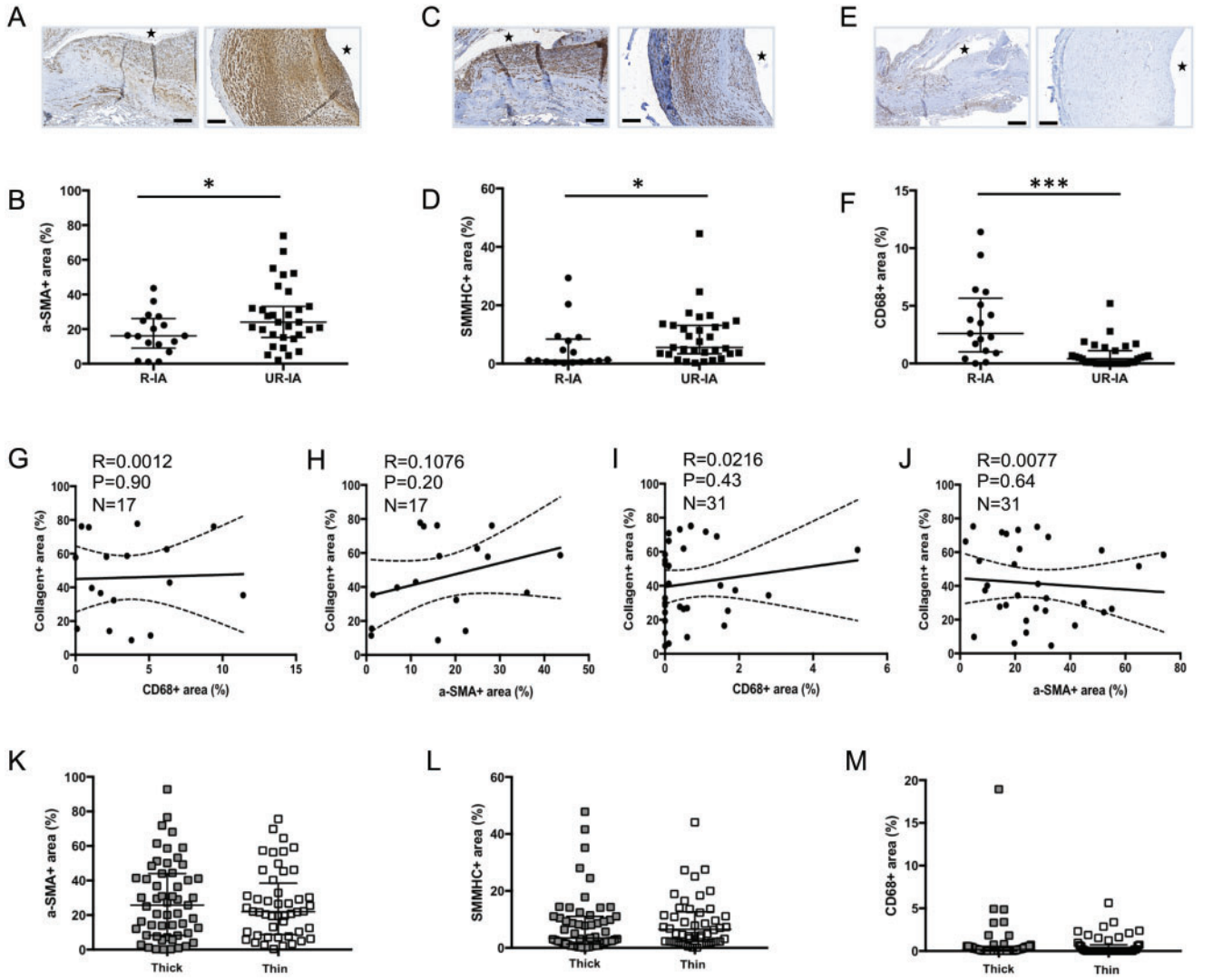

FIGURE 4. Cellular content of ruptured and unruptured intracranial aneurysms (IAs). Representative examples and quantification of α-SMA (SMCs in brown, **A, B**), SMMHCs (differentiated SMCs in brown, **C, D)** and CD68 (macrophages in brown, **E, F**) in ruptured and unruptured IA domes. Total collagen content is not correlated with CD68 **(G, I)** or α-SMA **(H, J)** contents in R-IAs (**G**, **H**) and UR-IAs **(I, J)**. Total SMC **(K)**, differentiated SMC **(L)** and macrophage **(M)** contents are not affected by the thickness of the aneurysmal wall in UR-IAs. The lumen of the vessel is indicated by a star. Results are shown as individual values and as median ± interquartile range. *$p \leq 0.05$, ***$p < 0.001$, nonparametric Mann-Whitney *U* test. Scale bars: **A**, **C**, **E** = 100 μm.

between age, sex or blood pressure and any of the histological IA wall characteristics.

DISCUSSION

The pathogenesis of IA formation and growth is complex and the precise biomechanical processes leading to aneurysmal wall rupture are not yet understood. The goal of our study was to characterize the aneurysmal wall histologically and to correlate histological characteristics with clinical and radiological factors used to estimate the risk of IA rupture. By establishing a new biobank of IA domes from patients surgically treated at the Geneva University Hospitals, we have unequivocally demonstrated that IA walls prone to rupture present a lower content in SMCs and collagen, a higher content in macrophages but no difference in elastin content (Figs. 2, 4). These results are in agreement with previously published studies performed in Japanese (11) or Finnish (12) cohorts. In addition, we showed that collagen content is different depending of the thickness of the IA wall in unruptured IAs, whereas no such difference was found in ruptured aneurysms (Fig. 3). Aneurysm dome classification, based on the histological score defined by Frösen et al (12), revealed a significant increased percentage of degenerative histological phenotypes (grades c and d) of ruptured IA walls compared with walls of unruptured IAs (Fig. 5). Finally, novel associations between histological characteristics of the IA wall and 3 clinical risk factors have been found. First, large size IAs have higher total collagen, type III collagen and macrophage contents; second, high content of type III collagen is associated

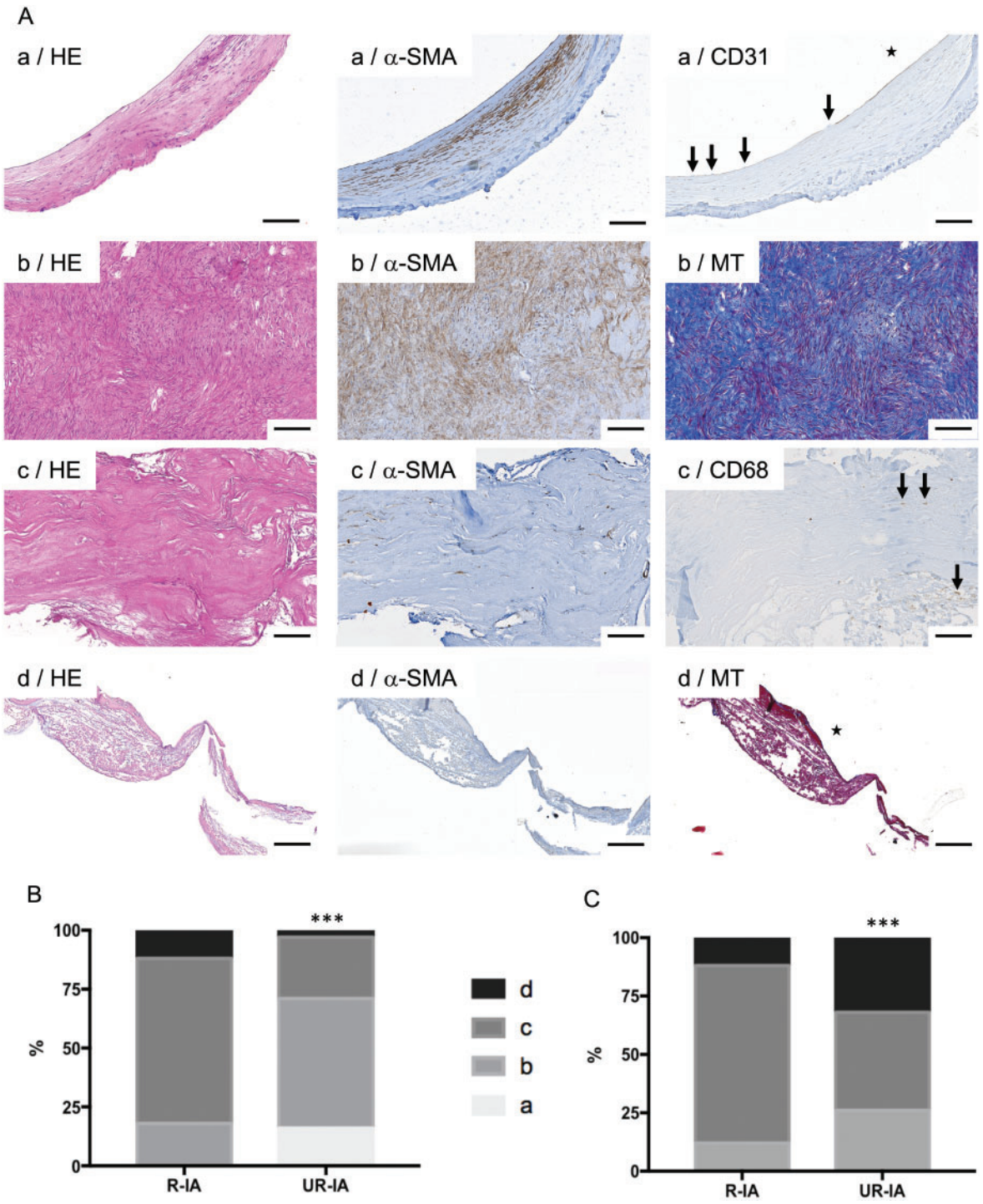

FIGURE 5. Classification of ruptured and unruptured intracranial aneurysms (IAs) based on histological characteristics. **(A)** Representative examples of stainings allowing IA histological classification following the definitions: **(a)** Endothelialized wall with linearly organized SMCs (first row); **(b)** Thickened wall with disorganized SMC (second row); **(c)** Hypocellular wall with either intimal hyperplasia or organizing luminal thrombosis (third row), and **(d)** An extremely thin thrombosis-lined hypocellular wall (fourth row). Scale bars: 100 μm. HE: hematoxylin and eosin staining; α-SMA: α-smooth muscle actin immunostaining (SMCs in brown); CD31: endothelial cell staining (in brown, endothelium indicated by arrows); MT: Masson-trichrome staining (collagen in blue); CD68: macrophage staining (in brown, some macrophages are indicated by arrows). The lumen of the vessel is indicated by a star. **(B, C)** Classification of ruptured and unruptured IAs following the (**a,** very light gray), (**b,** light gray), (**c,** dark grey) and (**d,** black) classification based on the dominant wall type **(B)** or on the most pathological region **(C)** observed in the resected sample. ***$p < 0.001$, Chi-square test.

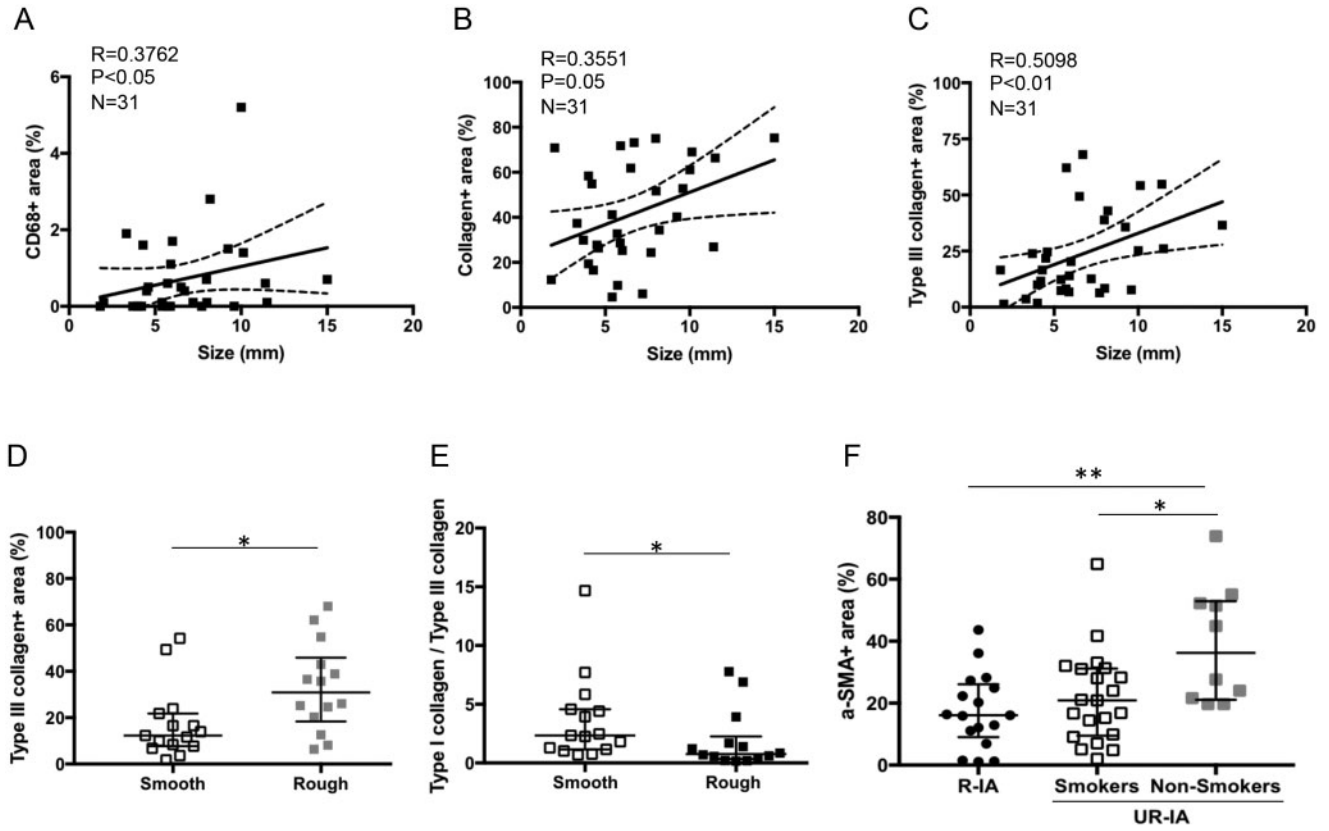

FIGURE 6. Risk factors and aneurysmal wall composition. Spearman correlation between intracranial aneurysm (IA) size and CD68 **(A)**, total collagen **(B)**, and type III collagen **(C)** contents in UR-IAs. UR-IAs with a rough appearance have a higher content of type III collagen **(D)** and a lower type I collagen-type III collagen ratio **(E)** than UR-IA with a smooth appearance ($n = 15$ and 14, respectively, $^*p < 0.05$, nonparametric Mann-Whitney *U* test). SMC content is lower in the unruptured aneurysmal wall of smokers (current and former) in comparison to nonsmokers (**F**, $n = 17$ for R-IA, $n = 21$ for UR-IA/smokers, and $n = 10$ for UR-IA/nonsmokers, $^*p < 0.05$, $^{***}p < 0.001$, nonparametric Mann-Whitney *U* test).

with increased aneurysm dome roughness; and third, SMC content is lower in unruptured IA walls of smokers (Fig. 6).

ECM components are constantly being synthesized and degraded in the arterial wall. ECM produced by SMCs and fibroblasts contributes to the maintenance of the structural integrity of the IA wall, whereas proteases and other matrix degrading enzymes secreted by inflammatory cells demolish ECM and destabilize the IA wall. In both ruptured and unruptured IAs we did not observe any correlation between α-SMA-positive cells and the total collagen content or the type I or type III collagen content (Fig. 4). An earlier study comparing the IA wall with the normal vessel wall of intracranial arteries demonstrated that medial SMCs in IAs switch to a synthetic phenotype characterized by a decreased expression of α-SMA and SMMHCs, the disappearance of smoothelin and an increased expression of S100A4 (22). S100A4 is a protein known to favor degradation and remodeling of the ECM by modulation of proteolytic activity (23, 24), and it has been proposed that S100A4 could, in part, play a role in the remodeling process observed in IAs (22). Immunostainings for α-SMA and SMMHCs performed on our samples to distinguish subpopulations of SMCs showed that SMCs were less abundant and less differentiated in ruptured IAs (Fig. 4) but no difference in the proportion of dedifferentiated SMCs between ruptured and unruptured IAs were observed. As elective IA treatment requires a critical size or growth of the aneurysm, our patient population is likely biased towards more advanced disease stages and the switch to the synthetic SMC phenotype might have already occurred during the initiation phase or early stages of the disease. However, we observed a lower collagen content in the wall of ruptured IAs compared with unruptured aneurysms. ECM degradation is induced by secretion of various metalloproteinases (MMPs) by inflammatory cells but also by resident vascular cells (25). Infiltrated tissular macrophages secrete, among others, MMP-2 and MMP-9 known to digest type I and III collagen fibers (26). Type I and III collagen fibers are important structural components of cerebral arteries. Whereas type I collagen plays a key role in the support of high tensile strength, type III collagen is an important regulatory element in type I collagen fibrillogenesis (27). Indeed, premature vascular aneurysms and fragility of cerebral arteries are associated with genetic mutations in type I and III collagen (28, 29). Furthermore, an increased activity and/or expression of MMP-2 and MMP-9 has been previously shown in ruptured IAs (compared with unruptured IAs) (26). In agreement with this observation, our study revealed lower

contents of both type I and type III collagen fibers in R-IAs. However, we did not find a direct correlation between CD68-positive cells and collagen contents (total, type I or III), thus the decrease of collagen content in ruptured IAs cannot be attributed to a specific type of cells but rather seems to be the consequence of the concomitant reduction in SMCs and the increase in macrophages in R-IAs. Of note, >60% of the IA domes have been resected <2 days after the first clinical symptoms of IA rupture, suggesting that a large part of the CD68-positive cells present in the aneurysmal wall were already infiltrated before the rupture, as already described by others (30).

Type III collagen is important for type I collagen fibrillogenesis (27) and deficiency or mutation of type III collagen have been described to favor IAs (28, 29). In our study, we confirmed that R-IAs have a lower content of type I and III collagen fibers; however, the overall ratio type III/type I is not different between the 2 groups (Fig. 2). Histologically, thin regions in UR-IAs appeared to be associated with a different relative contribution of type III and type I collagen in comparison to thicker wall regions of such IAs. In addition, we show that a clinical rough appearance of IAs associates with a higher content in type III collagen fibers in histology. As previous studies have pointed to the importance of collagen expression and organization in aneurysm wall strength (31) or regional wall shear stress (32), our observation provides a histological validation for the use of the rough appearance of the IA and urges towards further studies providing mechanistic insight in the critical relation between collagen subtype, the presence of submillimetric irregularities, blebs/lobules and risk of IA rupture.

Following the classification established by Frösen et al (12) for dominant wall type, we observed that ruptured IAs are in vast majority (82%) histologically characterized by hypocellular and/or very thin vascular walls and luminal thrombosis (grades c and d). In contrast, 71% of unruptured IA samples contain endothelial cells and/or a thickened media with SMCs. Furthermore, an important clinical risk factor for IA rupture, that is, smoking, was histologically associated with reduced SMC content in UR-IAs. In fact, the SMC content in UR-IAs of smokers was similar to the one found in R-IAs, suggesting that smoking enhances the process of IA degeneration thereby enhancing the risk of rupture. In support with this hypothesis, Starke et al showed recently in cultured cerebral vascular SMCs that cigarette smoke exposure increased NOX1 expression followed by an upregulation of pro-inflammatory/matrix remodeling genes and downregulation of contractile genes such as α-SMA and SMMHCs (33). For clinical practice, it will be difficult to develop specific radiological markers recognizing a hypocellular thin wall for the identification of IAs at high risk of rupture. In contrast, it might be a more fruitful approach to aim for the development of a SMC-related marker to identify the IAs at low risk to better stratify patients for (no) intervention.

An important limitation of our study is the relatively small number of patients. By comparing characteristics of patients and aneurysm in different outcomes groups of large cohorts, clinicians identified risk factors and estimate the rupture probability using scores integrating multiple variables (ISUIA [6], UCAS [5], PHASES [4], UIATS [3]). Histological studies open an avenue to better understand the mechanisms and progression of the disease and could reveal bio-markers to improve the estimation of risk. To rapidly progress in the field, it is of paramount importance to agree on standard operating procedures and reporting globally to better allow meta-analysis and pooling of individual studies or data. The associations found in our study between presently available clinical/radiological data such as IA size, rough appearance, smoking and specific histological characteristics underline once more the importance of combining clinical and histological data. Recent developments in augmented reality assisted surgery allow the precise mapping of aneurysm dome characteristics (34). Aneurysm wall aspects as observed during surgical interventions can be associated to particular lumen shape features or imaging characteristics observed as clinical markers and bridged to immuno-histological characteristics giving insights on the vessel wall constitution and remodeling. These developments will further strengthen the possible use of histology-based clinical markers in aneurysm wall risk assessment in the near future.

ACKNOWLEDGMENTS

We thank Juhana Frösen (Associate Professor, Kuopio University Hospital, Kuopio, Finland) and Riikka Tulamo, MD, PhD (Helsinki University Hospital, Helsinki, Finland) for their valuable advice on the histological IA classification. We thank the Bioimaging Core Facility, Faculty of Medicine, University of Geneva for technical help. This work has been performed with the contribution of the Clinical Trial Unit, Faculty of Medicine, Geneva University Hospitals.

REFERENCES

1. Vlak MH, Algra A, Brandenburg R, et al. Prevalence of unruptured intracranial aneurysms, with emphasis on sex, age, comorbidity, country, and time period: A systematic review and meta-analysis. Lancet Neurol 2011;10:626–36
2. Schatlo B, Fung C, Fathi AR, et al. Introducing a nationwide registry: The Swiss study on aneurysmal subarachnoid haemorrhage (Swiss SOS). Acta Neurochir (Wien) 2012;154:2173–8
3. Etminan N, Brown RD, Jr., Beseoglu K, et al. The unruptured intracranial aneurysm treatment score: A multidisciplinary consensus. Neurology 2015;85:881–9
4. Greving JP, Wermer MJ, Brown RD, Jr., et al. Development of the PHASES score for prediction of risk of rupture of intracranial aneurysms: A pooled analysis of six prospective cohort studies. Lancet Neurol 2014; 13:59–66.
5. Investigators UJ, Morita A, Kirino T, et al. The natural course of unruptured cerebral aneurysms in a Japanese cohort. N Engl J Med 2012;366: 2474–82
6. Wiebers DO, Whisnant JP, Huston J, 3rd, et al. Unruptured intracranial aneurysms: Natural history, clinical outcome, and risks of surgical and endovascular treatment. Lancet 2003;362:103–10
7. Etminan N, Beseoglu K, Barrow DL, et al. Multidisciplinary consensus on assessment of unruptured intracranial aneurysms: Proposal of an international research group. Stroke 2014;45:1523–30
8. Kotowski M, Naggara O, Darsaut TE, et al. Safety and occlusion rates of surgical treatment of unruptured intracranial aneurysms: A systematic review and meta-analysis of the literature from 1990 to 2011. J Neurol Neurosurg Psychiatry 2013;84:42–8
9. Naggara ON, Lecler A, Oppenheim C, et al. Endovascular treatment of intracranial unruptured aneurysms: A systematic review of the literature on safety with emphasis on subgroup analyses. Radiology 2012;263: 828–35

10. Darsaut TE, Findlay JM, Magro E, et al. Surgical clipping or endovascular coiling for unruptured intracranial aneurysms: A pragmatic randomised trial. J Neurol Neurosurg Psychiatry 2017;88:663–8
11. Kataoka K, Taneda M, Asai T, et al. Structural fragility and inflammatory response of ruptured cerebral aneurysms. A comparative study between ruptured and unruptured cerebral aneurysms. Stroke 1999;30: 1396–401
12. Frosen J, Piippo A, Paetau A, et al. Remodeling of saccular cerebral artery aneurysm wall is associated with rupture: Histological analysis of 24 unruptured and 42 ruptured cases. Stroke 2004;35:2287–93
13. Tulamo R, Frosen J, Junnikkala S, et al. Complement activation associates with saccular cerebral artery aneurysm wall degeneration and rupture. Neurosurgery 2006;59:1069–76
14. Frosen J, Tulamo R, Heikura T, et al. Lipid accumulation, lipid oxidation, and low plasma levels of acquired antibodies against oxidized lipids associate with degeneration and rupture of the intracranial aneurysm wall. Acta Neuropathol Commun 2013;1:71
15. Ollikainen E, Tulamo R, Frosen J, et al. Mast cells, neovascularization, and microhemorrhages are associated with saccular intracranial artery aneurysm wall remodeling. J Neuropathol Exp Neurol 2014; 73:855–64
16. Korkmaz E, Kleinloog R, Verweij BH, et al. Comparative ultrastructural and stereological analyses of unruptured and ruptured saccular intracranial aneurysms. J Neuropathol Exp Neurol 2017;76:908–16
17. Hirsch S, Bijlenga P. Shape? Shape. Shape! Pan Eur Netw: Sci Technol 2016;18:178–81
18. Dunlop R, Arbona A, Rajasekaran H, et al. @neurIST – chronic disease management through integration of heterogeneous data and computer-interpretable guideline services. Stud Health Technol Inform 2008;138: 173–7
19. Gondar R, Gautschi OP, Cuony J, et al. Unruptured intracranial aneurysm follow-up and treatment after morphological change is safe: Observational study and systematic review. J Neurol Neurosurg Psychiatry 2016; 87:1277–82
20. Bijlenga P, Ebeling C, Jaegersberg M, et al. Risk of rupture of small anterior communicating artery aneurysms is similar to posterior circulation aneurysms. Stroke 2013;44:3018–26
21. Skalli O, Ropraz P, Trzeciak A, et al. A monoclonal antibody against alpha-smooth muscle actin: A new probe for smooth muscle differentiation. J Cell Biol 1986;103:2787–96
22. Coen M, Burkhardt K, Bijlenga P, et al. Smooth muscle cells of human intracranial aneurysms assume phenotypic features similar to those of the atherosclerotic plaque. Cardiovasc Pathol 2013;22:339–44
23. Bresnick AR, Weber DJ, Zimmer DB. S100 proteins in cancer. Nat Rev Cancer 2015;15:96–109
24. Donato R, Cannon BR, Sorci G, et al. Functions of S100 proteins. Curr Mol Med 2013;13:24–57
25. Newby AC. Metalloproteinase expression in monocytes and macrophages and its relationship to atherosclerotic plaque instability. Arterioscler Thromb Vasc Biol 2008;28:2108–14
26. Kilic T, Sohrabifar M, Kurtkaya O, et al. Expression of structural proteins and angiogenic factors in normal arterial and unruptured and ruptured aneurysm walls. Neurosurgery 2005;57:997–1007
27. Liu X, Wu H, Byrne M, et al. Type III collagen is crucial for collagen I fibrillogenesis and for normal cardiovascular development. Proc Natl Acad Sci U S A1997;94:1852–6
28. Pope FM, Kendall BE, Slapak GI, et al. Type III collagen mutations cause fragile cerebral arteries. Br J Neurosurg 1991;5:551–74
29. Mohan D, Munteanu V, Coman T, et al. Genetic factors involves in intracranial aneurysms – actualities. J Med Life 2015;8:336–41
30. Frosen J, Tulamo R, Paetau A, et al. Saccular intracranial aneurysm: Pathology and mechanisms. Acta Neuropathol 2012;123:773–86
31. Robertson AM, Duan X, Aziz KM, et al. Diversity in the strength and structure of unruptured cerebral aneurysms. Ann Biomed Eng 2015;43: 1502–15
32. Cebral JR, Duan X, Gade PS, et al. Regional mapping of flow and wall characteristics of intracranial aneurysms. Ann Biomed Eng 2016;44: 3553–67
33. Starke RM, Thompson JW, Ali MS, et al. Cigarette smoke initiates oxidative stress-induced cellular phenotypic modulation leading to cerebral aneurysm pathogenesis. Arterioscler Thromb Vasc Biol 2018;38:610–21
34. Cabrilo I, Bijlenga P, Schaller K. Augmented reality in the surgery of cerebral aneurysms: A technical report. Neurosurgery 2014;10(Suppl. 2): 252–60